QUANTUM IMAGING

Quantum reference beacon–guided superresolution optical focusing in complex media

Donggyu Kim[1,2]* and Dirk R. Englund[2,3]

Optical scattering is generally considered to be a nuisance of microscopy that limits imaging depth and spatial resolution. Wavefront shaping techniques enable optical imaging at unprecedented depth, but attaining superresolution within complex media remains a challenge. We used a quantum reference beacon (QRB), consisting of solid-state quantum emitters with spin-dependent fluorescence, to provide subwavelength guidestar feedback for wavefront shaping to achieve a superresolution optical focus. We implemented the QRB-guided imaging with nitrogen-vacancy centers in diamond nanocrystals, which enable optical focusing with a subdiffraction resolution below 186 nanometers (less than half the wavelength). QRB-assisted wavefront-shaping should find use in a range of applications, including deep-tissue quantum enhanced sensing and individual optical excitation of magnetically coupled spin ensembles for applications in quantum information processing.

Optical random scattering in complex media, such as biological tissue, distorts an incident optical focus, reducing the resolution and imaging depth of optical microscopy. However, random scattering need not lead to the permanent loss of focusing capability; instead, it randomizes the incident focus in a deterministic way. By reversing this scattering, focusing (*1*, *2*) and imaging (*3*–*5*) through complex media become possible. Moreover, random scattering can actually benefit microscopy (*1*, *2*, *4*, *5*) by permitting a spatial resolution below the diffraction limit of $\lambda/2NA$, where λ is the wavelength and NA is the numerical aperture of the microscope objective. This superresolution is possible because random scattering couples optical modes with high in-plane momentum from the sample to the microscope objective, much like a disordered grating. By extending this principle to evanescent modes of the sample, far-field superlenses for near-field focusing (*2*) and imaging (*5*) have been achieved.

Reversing random scattering requires feedback from the target focal points. In particular, focusing light inside of complex media requires a type of guidestar (GS) that provides feedback of the interior optical field (*6*). This feedback guides incident wavefront adjustments to focus the scattered light into the GS point. Various forms of GSs have been implemented, including fluorescence (*7*), ultrasound (*8*–*13*), nonlinear reference beacons (*14*), and kinetic objects (*15*, *16*). However, the spatial resolution when using these types of GSs has been far from the superresolution limit (*6*). To push this resolution to or below the diffraction limit requires two key advances: (i) The physical size of the GS needs to be of subwavelength scale, and (ii) resolving subdiffraction features of randomly scattered light must be possible (*2*, *5*). A subwavelength aperture used in scanning near-field optical microscopy (SNOM) satisfies these conditions, but this technique does not permit imaging within a complex medium.

We introduce quantum reference beacons (QRBs), which consist of solid-state quantum emitters with spin-dependent fluorescence. An example is the nitrogen vacancy (NV) center in diamond, which has emerged as a leading quantum system for quantum sensing (*17*, *18*) and quantum information processing (*19*–*23*). By resonantly driving electron spin transitions of each QRB, the spin-dependent fluorescence produces the subwavelength GS feedback that enables superresolution focusing within complex media.

In our approach to QRB-guided wavefront shaping in microscopy (Fig. 1), a wavefront shaper adjusts basis modes (shown as individual pixels in Fig. 1A) of the incident wavefront to interfere scattered light constructively at target GS points. This specific wavefront adjustment is determined from the QRB-GS feedback. This feedback signal is created by applying a magnetic field gradient across the sample so that one of several QRBs inside a diffraction-limited volume can be selectively driven into its dark magnetic sublevels (Fig. 1C).

Specifically, the QRB-GS feedback signal is needed to measure the transmission matrix (*6*) that characterizes the light propagation through a complex medium (*24*). We labeled the electron spin state of the embedded QRBs at $\{\mathbf{x}_i\} = \mathbf{x}_1, \ldots, \mathbf{x}_N$, with a spin density operator $\boldsymbol{\rho} = \rho_1 \otimes \rho_2 \otimes \cdots \otimes \rho_N$. An external magnetic field gradient separates their resonance frequencies $\{v_i\}$ by the Zeeman effect. In principle, $\{\mathbf{x}_i\}$ could then be reconstructed from $\{v_i\}$ and knowledge of the external magnetic field gradient. Resonant driving of each $\{\rho_i\}$ spin transition is represented through a quantum operator $\{E_i\}$. When the jth incident basis mode is coupled into the medium, the QRB-GS feedback $S_{i,j}$ for $\mathbf{x}_i$ is described by

$$S_{i,j} = N_j[\boldsymbol{\rho}] - N_j[E_i(\boldsymbol{\rho})] = |t_{i,j}|^2 \Delta\sigma_i \Delta\gamma \qquad (1)$$

Here, $N_j[\boldsymbol{\rho}]$ and $N_j[E_i(\boldsymbol{\rho})]$ denote the fluorescence photon numbers collected for unit integration; $t_{i,j}$ is the transmission matrix element (the scattered optical field at $\mathbf{x}_i$ for the jth incident basis mode); $\Delta\sigma_i = \frac{1}{2}\mathrm{tr}\{\sigma_z[\rho_i - E_i(\rho_i)]\}$, where σ_z is the Pauli-z operator; and $\Delta\gamma$ represents the variance of the collected spin-dependent fluorescence between the optically bright and dark spin states (Fig. 1B). The iterative wavefront adjustments due to the QRB-GS feedback are summarized in Fig. 2.

The spatial resolution of our method is determined by the electron spin resonance (ESR) lineshape (*24*) because the lineshape sets the point spread function (PSF) of the QRB-GS feedback that confines $\{E_i\}$ only to the target QRBs (Fig. 2A). A magnetic field gradient dB/dx translates the (mean) resonance linewidth δv to the spatial resolution Δd_{QRB} of the effective PSF

$$\Delta d_{\mathrm{QRB}} = \frac{\delta v}{\gamma_e (dB/dx)} \qquad (2)$$

where γ_e is the gyromagnetic ratio of the electronic spin (≃2.8 MHz/Gauss). Combined with the crystal orientation–dependent Zeeman splitting and dynamical decoupling to narrow the linewidth, this resolution can go down to a few tens of nanometers (*25*, *26*).

In the experimental configuration for demonstrating QRB-assisted wavefront shaping (Fig. 3), our QRBs consist of ensembles of NV centers (Fig. 1B) in nanodiamonds with a mean diameter of 50 nm. The QRBs are embedded in a complex medium consisting of randomly distributed TiO_2 nanoparticles with a mean diameter of 21 nm. The incident green laser light (λ = 532 nm) is randomly scattered as it propagates through the medium. This scattering produces subwavelength spatial features on the incident laser light (*2*), which excite the embedded QRBs. In particular, we demonstrate superresolution focusing on two QRBs at $\mathbf{x}_1$ (QRB_1) and $\mathbf{x}_2$ (QRB_2) in Fig. 3B, where their separation $|\mathbf{x}_1 - \mathbf{x}_2|$ = 186 nm is far below the diffraction limit of our excitation objective lens, 406 nm (fig. S3). The QRB_1 has the ESR frequency of v_1 = 2.825 GHz, and the QRB_2 has the ESR frequency of v_2 = 2.762 GHz, which corresponds to the electronic spin transition between $|m_s = 0\rangle$ and one of the Zeeman-split $|m_s = \pm 1\rangle$ of the ground spin triplet ($^3A_2$) (Fig. 1B). Because v_1 and v_2 are well separated ($\Delta v \simeq 63$ MHz) compared with their resonance linewidths (δv_1 = 5 MHz and δv_2 = 5.6 MHz), it is possible to individually drive the spin transition of each QRB.

[1]Department of Mechanical Engineering, Massachusetts Institute of Technology, 77 Massachusetts Avenue, Cambridge, MA 02139, USA. [2]Research Laboratory of Electronics, Massachusetts Institute of Technology, 50 Vassar Street, Cambridge, MA 02139, USA. [3]Department of Electrical Engineering and Computer Science, Massachusetts Institute of Technology, 50 Vassar Street, Cambridge, MA 02139, USA.
*Corresponding author. E-mail: donggyu@mit.edu

We shaped the incident wavefront with 793 transverse Fourier basis modes $\{\mathbf{k}_n\}$, which cover the entire back aperture of the excitation objective. Resonant microwaves drive the spin transitions at v_1 and v_2 that produce the QRB-GS feedback, and the phase of $\{\mathbf{k}_n\}$ is iteratively adjusted to optimize the feedback signal (Fig. 2, D and F). The results of the wavefront optimizations W_{v_1} and W_{v_2} are plotted in Fig. 4, A and B, respectively. For comparison, the wavefront W_{cl}, obtained without the use of ESR (by optimizing only fluorescence feedback from QRBs), is shown in Fig. 4C. This fluorescence GS method (*6*, *7*) focuses the interior optical field without achieving superresolution.

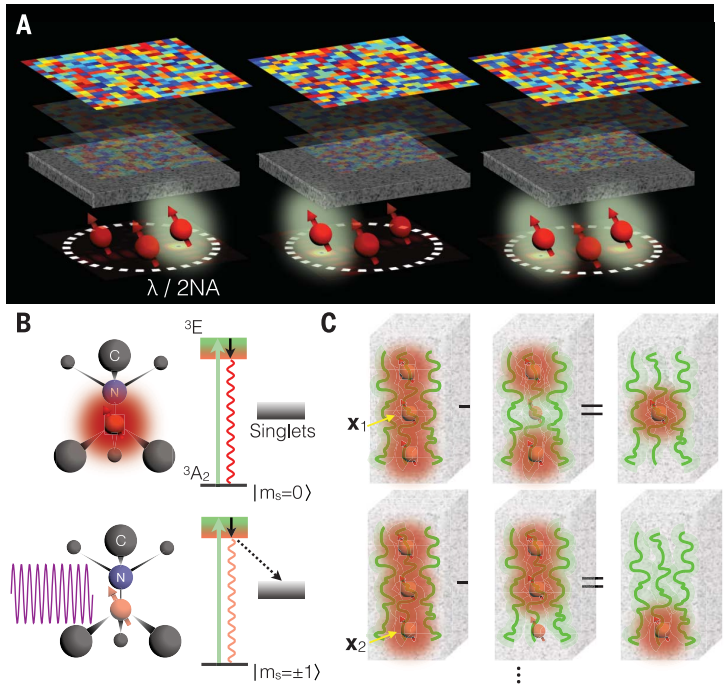

Fig. 1. Wavefront shaping guided by QRBs. (**A**) Optical random scattering in complex media distorts the incident optical field. However, this distortion can be reversed by shaping the incident wavefront. Embedded QRBs provide feedback about subwavelength features of the scattered optical fields, guiding the wavefront-shaping process. This approach enables, for example, superresolution focusing deep inside of complex media or individual spin-qubit measurement in a diffraction-limited area (dashed circle). (**B**) NV centers in diamond with spin-dependent fluorescence. Electrons with the spin magnetic sublevels $|m_s = \pm1\rangle$ preferentially decay (dashed black arrow) to the dark metastable singlets once they are optically pumped to the excited states ^{3}E (green arrow), resulting in reduced fluorescence than that from the sublevel $|m_s = 0\rangle$. This spin-dependent fluorescence enables ODMR. (**C**) The QRB-GS feedback is produced with the spin-dependent fluorescence. To measure the optical field on the QRB positioned at $\mathbf{x}_1$, its fluorescence is selectively reduced by means of ESR. The change of collected fluorescence determines the optical field at $\mathbf{x}_1$. This process can be repeated for another position at $\mathbf{x}_2$, as shown in the bottom plot.

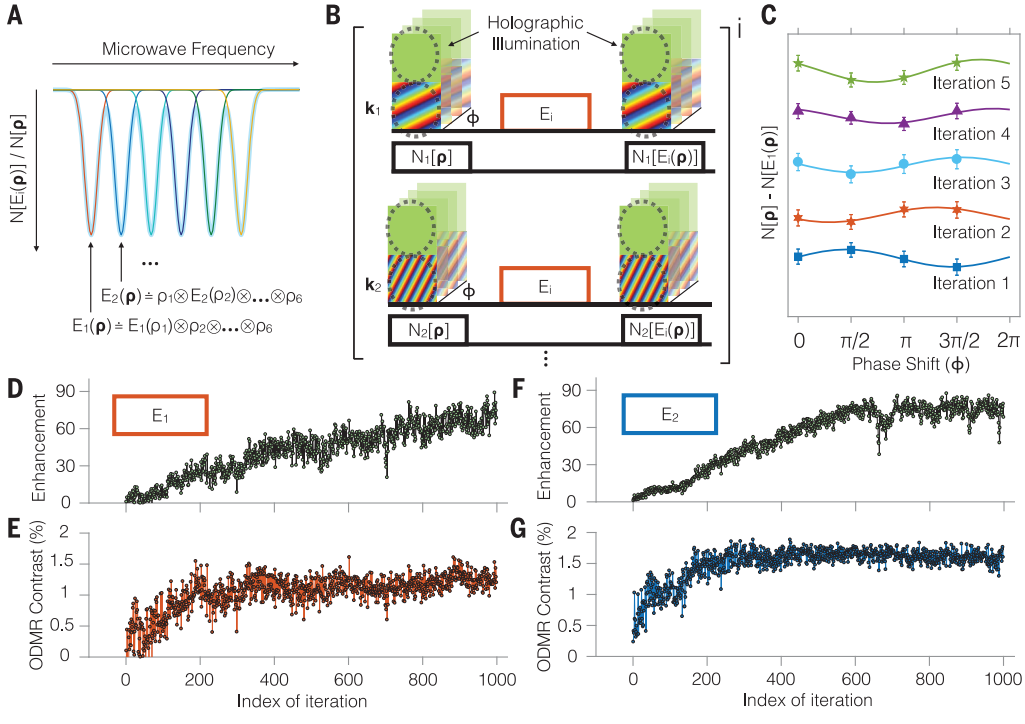

Fig. 2. Iterative wavefront optimization with QRB-GS feedback. (**A**) $\{\rho_i\}$ label the electron spin states of QRBs, and an external magnetic field gradient splits their individual resonance frequencies. Quantum operators $\{E_i\}$ drive the electron spin transition of target QRBs. (**B**) Measurement sequences for the iterative wavefront optimization. The Fourier basis modes of the incident wavefront ($\mathbf{k}_1$, $\mathbf{k}_2$, ...) are encoded into holographic illuminations, in which the basis modes interfere with the reference plane wave for complex field readout (*24*). The overall fluorescence difference with $\{E_i\}$, $N_j[\boldsymbol{\rho}] - N_j[E_i(\boldsymbol{\rho})]$, produces the QRB-GS feedback $S_{i,j}$. ϕ describes the phase of each basis mode relative to the reference plane wave. (**C**) Modulation of the QRB-GS feedback in the iterative wavefront optimization. In each step, the phase ϕ of the basis modes is adjusted to compensate for the phase offset of the modulation. (**D** and **F**) The iterative wavefront optimization with the QRB-GS feedback. Two QRBs have the electron spin resonance frequencies at v_1 = 2.825 GHz and v_2 = 2.762 GHz. The resonant microwaves continuously drive the resonances to produce the QRB-GS feedback, so that the incident optical fields can be iteratively updated to optimize the QRB-GS feedback signal strength. (**E** and **G**) The ODMR contrast at v_1 and v_2 for the iterative optimization processes. Each iteration of the optimization process required 48 s (fig. S1).

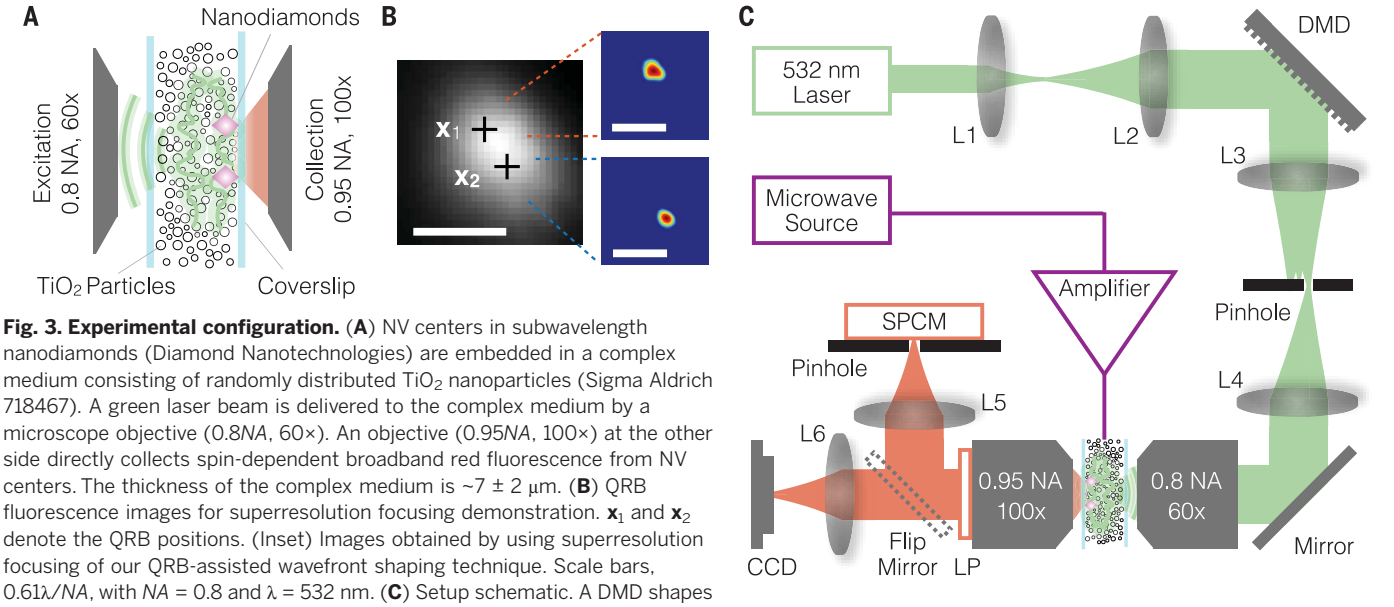

Fig. 3. Experimental configuration. (**A**) NV centers in subwavelength nanodiamonds (Diamond Nanotechnologies) are embedded in a complex medium consisting of randomly distributed TiO_2 nanoparticles (Sigma Aldrich 718467). A green laser beam is delivered to the complex medium by a microscope objective (0.8*NA*, 60×). An objective (0.95*NA*, 100×) at the other side directly collects spin-dependent broadband red fluorescence from NV centers. The thickness of the complex medium is ~7 ± 2 μm. (**B**) QRB fluorescence images for superresolution focusing demonstration. $\mathbf{x}_1$ and $\mathbf{x}_2$ denote the QRB positions. (Inset) Images obtained by using superresolution focusing of our QRB-assisted wavefront shaping technique. Scale bars, $0.61\lambda/NA$, with $NA = 0.8$ and $\lambda = 532$ nm. (**C**) Setup schematic. A DMD shapes the wavefront of the incident green laser and projects it onto the back aperture of the excitation objective. The phase of each incident basis mode $\{\mathbf{k}_n\}$ is controlled by groups of 24-by-24 DMD micromirrors. A single photon-counting module (SPCM) detects the red fluorescence collected by the collection objective, and a charge-coupled device (CCD) captures fluorescence images. A long-pass optical filter with a cutoff wavelength of 650 nm (LP) rejects the green laser, and a pinhole in front of the SPCM blocks stray red fluorescence. A copper wire (diameter of 25 μm) delivers the microwave signal to QRBs to modulate their spin ground state population. A permanent magnet (not shown) separates the magnetic resonance frequencies of the QRBs by means of orientation-dependent Zeeman splitting. L1 to L6 indicate lenses.

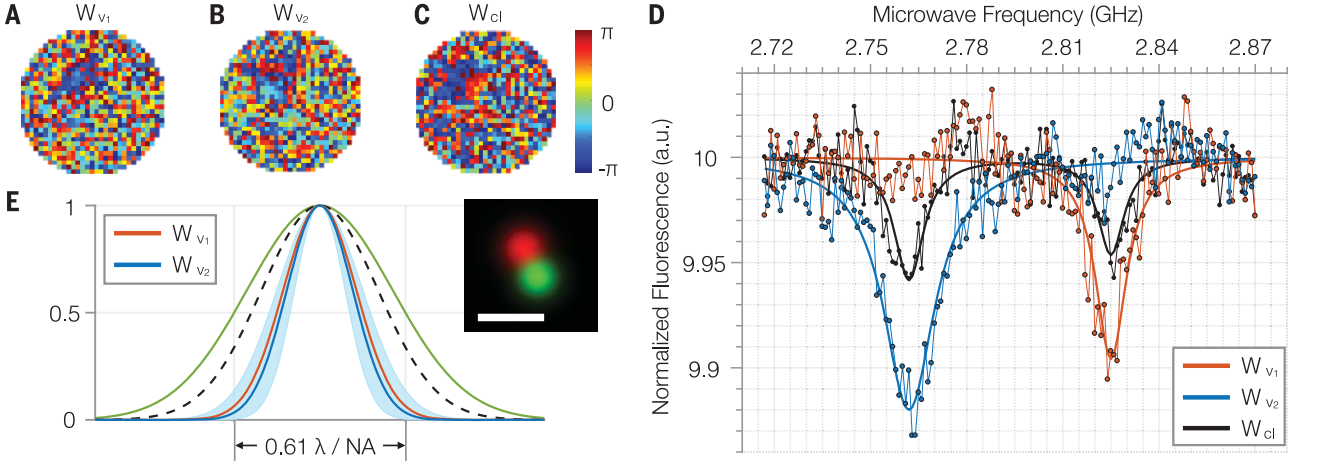

Fig. 4. Subwavelength optical focusing in a complex medium. (**A** and **B**) The phase-only wavefronts W_{v_1} and W_{v_2}, determined by optimizing the QRB-GS feedback at v_1 and v_2, respectively. (**C**) The phase-only wavefront W_{cl}, obtained by using the fluorescence GS method. (**D**) ODMR spectra with W_{v_1} (red), W_{v_2} (blue), and W_{cl} (black) projection. (**E**) Spatial resolution of the subwavelength foci in the complex medium. The red and blue lines plot the estimated intensity shape of the subwavelength foci with W_{v_1} and W_{v_2} projection, respectively. The shaded area gives the estimation uncertainty. The green line plots the PSF of the excitation objective (full width at half maximum = $0.61\lambda/NA$, with $\lambda = 532$ nm and $NA = 0.8$), and the black dashed line refers to the far-field limited PSF ($NA = 1$). (Inset) Reconstructed image of the subwavelength foci, with W_{v_1} (red) and W_{v_2} (green). Scale bar, $0.61\lambda/NA$, with $NA = 0.8$ and $\lambda = 532$ nm.

Projecting the wavefronts W_{v_1} and W_{v_2} forms a superresolution optical focus at $\mathbf{x}_1$ and $\mathbf{x}_2$, respectively, in the complex medium. We can verify this superresolution focusing by investigating optically detectable magnetic resonance (ODMR) spectra. This is possible because ODMR spectra exhibit resonances only of optically pumped QRBs, and QRB_1 and QRB_2 have distinguishable spectra. The ODMR spectra for this investigation are plotted in Fig. 4D. First, we projected the wavefront W_{cl} with the digital micromirror device (DMD), which produces the ODMR spectrum shown in Fig. 4D as the black line. This spectrum shows the resonances at v_1 and v_2 of both QRBs, as expected. By contrast, the only resonance of QRB_1 appears (Fig. 4D, red line) when we project W_{v_1}, which we obtained using the QRB-GS feedback with the spin transition at v_1. Alternatively, projecting W_{v_2} reveals the resonance of QRB_2 (Fig. 4D, blue line). This demonstration validates the ability of QRB-guided wavefront shaping to enable optical addressing of individual spots far below the diffraction limit.

The ODMR spectra with subwavelength spin addressing enabled us to estimate the spatial resolutions of the optical foci (Fig. 4E). We

determined the peak-to-background intensity ratio of the focus [$I(\mathbf{x}_1)/I(\mathbf{x}_2)$ or vice versa] from the ODMR spectra (*24*). Assuming the subwavelength focus features a Gaussian intensity envelope, the intensity ratio indicates that the superresolution focus at $\mathbf{x}_1$ has a spatial resolution of 204 nm and at $\mathbf{x}_2$ has a spatial resolution of 184 nm. This achieved resolution is for $\mathbf{x}_1$ and $\mathbf{x}_2$, respectively, 2 and 2.21 times smaller than our diffraction-limited resolution and 1.31 and 1.45 times smaller than the far field–limited one (NA = 1).

QRBs enable superresolution optical focusing within complex media. This QRB-GS approach distinctly provides subwavelength GS feedback inside a complex medium by the use of spin coherence. QRB-assisted wavefront shaping opens up a range of applications: It can extend to quantum sensing based on NV centers to greater imaging depth and optical superresolution; it can also be used to characterize the light propagation through a fiber for single-fiber endomicroscopy (*27*). Our method could open up the way for subwavelength optical spin measurement (*28*, *29*) of magnetic dipole-coupled quantum emitters (*25*), which is essential for advanced quantum sensing (*30*), quantum error correction (*21*), and room-temperature quantum computing (*31*).

REFERENCES AND NOTES

1. I. M. Vellekoop, A. Lagendijk, A. Mosk, *Nat. Photonics* **4**, 320–322 (2010).
2. J.-H. Park *et al.*, *Nat. Photonics* **7**, 454–458 (2013).
3. S. Popoff, G. Lerosey, M. Fink, A. C. Boccara, S. Gigan, *Nat. Commun.* **1**, 81 (2010).
4. Y. Choi *et al.*, *Phys. Rev. Lett.* **107**, 023902 (2011).
5. C. Park *et al.*, *Phys. Rev. Lett.* **113**, 113901 (2014).
6. R. Horstmeyer, H. Ruan, C. Yang, *Nat. Photonics* **9**, 563–571 (2015).
7. I. M. Vellekoop, E. G. van Putten, A. Lagendijk, A. P. Mosk, *Opt. Express* **16**, 67–80 (2008).
8. X. Xu, H. Liu, L. V. Wang, *Nat. Photonics* **5**, 154–157 (2011).
9. K. Si, R. Fiolka, M. Cui, *Nat. Photonics* **6**, 657–661 (2012).
10. Y. M. Wang, B. Judkewitz, C. A. Dimarzio, C. Yang, *Nat. Commun.* **3**, 928 (2012).
11. B. Judkewitz, Y. M. Wang, R. Horstmeyer, A. Mathy, C. Yang, *Nat. Photonics* **7**, 300–305 (2013).
12. T. Chaigne *et al.*, *Nat. Photonics* **8**, 58–64 (2014).
13. P. Lai, L. Wang, J. W. Tay, L. V. Wang, *Nat. Photonics* **9**, 126–132 (2015).
14. O. Katz, E. Small, Y. Guan, Y. Silberberg, *Optica* **1**, 170 (2014).
15. C. Ma, X. Xu, Y. Liu, L. V. Wang, *Nat. Photonics* **8**, 931–936 (2014).
16. H. Ruan, M. Jang, C. Yang, *Nat. Commun.* **6**, 8968 (2015).
17. G. Balasubramanian *et al.*, *Nature* **455**, 648–651 (2008).
18. G. Kucsko *et al.*, *Nature* **500**, 54–58 (2013).
19. H. Bernien *et al.*, *Nature* **497**, 86–90 (2013).
20. W. Pfaff *et al.*, *Science* **345**, 532–535 (2014).
21. T. H. Taminiau, J. Cramer, T. van der Sar, V. V. Dobrovitski, R. Hanson, *Nat. Nanotechnol.* **9**, 171–176 (2014).
22. G. Waldherr *et al.*, *Nature* **506**, 204–207 (2014).
23. N. Kalb *et al.*, *Science* **356**, 928–932 (2017).
24. Materials and methods are available as supplementary materials.
25. F. Dolde *et al.*, *Nat. Phys.* **9**, 139–143 (2013).
26. K. Arai *et al.*, *Nat. Nanotechnol.* **10**, 859–864 (2015).
27. Y. Choi *et al.*, *Phys. Rev. Lett.* **109**, 203901 (2012).
28. E. Rittweger, K. Y. Han, S. E. Irvine, C. Eggeling, S. W. Hell, *Nat. Photonics* **3**, 144–147 (2009).
29. P. Maurer *et al.*, *Nat. Phys.* **6**, 912–918 (2010).
30. V. Giovannetti, S. Lloyd, L. Maccone, *Nat. Photonics* **5**, 222–229 (2011).
31. N. Y. Yao *et al.*, *Nat. Commun.* **3**, 800 (2012).

ACKNOWLEDGMENTS

The authors thank N. H. Wan for helpful discussions. **Funding:** D.K. acknowledges financial support from the Kwanjeong Educational Foundation. This research is supported in part by the Army Research Office Multidisciplinary University Research Initiative (ARO MURI) biological transduction program and the NSF Center for Integrated Quantum Materials (DMR-1231319). **Author contributions:** D.K. and D.R.E. conceived the project, developed the theoretical formalism, and wrote the manuscript. D.K. designed and performed the experiments and analyzed the data. D.R.E. supervised the project. **Competing interests:** The superresolution method in this work was filed as a U.S. Provisional Patent Application (62/618297). **Data and materials availability:** All data needed to evaluate the conclusions in the paper are present in the paper and the supplementary materials.

SUPPLEMENTARY MATERIALS

www.sciencemag.org/content/363/6426/528/suppl/DC1
Materials and Methods
Supplementary Text
Figs. S1 to S3
References (*32*–*36*)

29 December 2017; accepted 26 February 2018
10.1126/science.aar8609

Quantum reference beacon–guided superresolution optical focusing in complex media

Donggyu Kim and Dirk R. Englund

Science **363** (6426), 528-531.
DOI: 10.1126/science.aar8609

Quantum beacons for enhanced imaging

Imaging an object is simply a case of collecting the light that is scattered from that object. However, if the object is embedded in or separated by a complex medium (tissue or atmosphere, for example), then the light is scattered, the wavefront of the light is muddled, and the image quality is reduced. Adaptive optics techniques use "guidestars" or "reference beacons" to undo the wavefront mixing and sharpen up the image. Kim and Englund show that nitrogen vacancy centers in diamond can be used as quantum reference beacons to enable superresolution focusing inside a scattering medium. The technique should be useful for quantum enhanced imaging and sensing applications.

Science, this issue p. 528